Multi-dimensional high energy density physics modeling and simulation of wire array Z-pinch physics[a)]

C. J. Garasi,[b)] D. E. Bliss, and T. A. Mehlhorn
Sandia National Laboratories, Albuquerque, New Mexico 87185

B. V. Oliver
Mission Research Corporation, Albuquerque, New Mexico 87110

A. C. Robinson
Sandia National Laboratories, Albuquerque, New Mexico 87185

G. S. Sarkisov
K-Tech Corporation, Albuquerque, New Mexico 87106

(Received 31 October 2003; accepted 22 December 2003; published online 23 April 2004)

The two- and three-dimensional (2D and 3D) versions of ALEGRA-HEDP [A. C. Robinson and C. J. Garasi, ''Three-dimensional Z-pinch wire array modeling,'' Computer Physics Communications, submitted] have been utilized to simulate discrete wire effects including precursor formation in 2D (r-θ plane) and nonuniform axial ablation (3D). Comparisons made between 2D and 3D simulations indicate that 2D simulations overestimate the mass ablation rate by a factor of 10–100 with respect to the 3D case, causing pre-mature motion of the array with respect to experimental data. Additionally, the 2D case advects a factor of 5 more current to axis than the 3D case. The integrity of the simulations is assessed by comparing the results to laser imaging of wire ablation and array trajectory information inferred from visible and x-ray imaging. Comparisons to previously proposed ablation models are also presented. These simulations represent the first high-fidelity three-dimensional calculations of wire-array pinch geometries. © *2004 American Institute of Physics.* [DOI: 10.1063/1.1683506]

I. INTRODUCTION

The implosion of centimeter-high cylindrical wire arrays via megaAmpere current drives has proven itself as an efficient means of converting electrical energy into x-ray radiation.[1–3] The radiation output from these arrays is relevant to the study of radiation–material interactions and ablator physics found within inertial confinement fusion (ICF) programs[4] as well as laboratory astrophysics studies.[5,6] Various wire array configurations have been proposed[7,8] in order to increase power output and meet requirements for ICF. Understanding how these arrays work and avenues for their optimization is critical to the success of ICF programs.

The development of models that adequately represent the various phases of current-driven wire array evolution requires the coordinated efforts of experimental, theoretical, and numerical approaches. The advent of more detailed experimental diagnostics and enhanced computer simulation methods have increased our understanding of the physics and dynamics associated with wire arrays.[9–11] Early models that assumed wire material explosion and evolution into unstable cylindrical shells of plasma during collapse have been replaced with more complex descriptions as enhanced radiation diagnostics are utilized to diagnose the state of the plasma.[12–14] Figures 1 and 2 illustrate the complexity of wire array evolution using laser shadowgraphy during wire initiation, subsequent wire merger, and the beginning of array implosion on the Z accelerator at Sandia National Laboratories. The images display nonuniform wire ablation in well-defined streams, injecting plasma pre-fill interior to the array before the bulk of the array collapses due to magnetic forces. Nonuniform wire ablation leads to nonuniform wire breakup and a loss of the well-defined streams. Nonuniform wire breaks provide a mechanism for some material to be left behind as the bulk array mass stagnates onto the pre-fill. Once the bulk material has stagnated, electrical current can shift back to the material left behind, causing it to stagnate onto the already collapsed bulk array mass.[11] These complex effects impact the total radiation output from the wire array and its application for ICF purposes.

Computational modeling of Z pinches has met with both success and failures.[15] Initially started in one dimension, moved to 2D cylindrical, and final progression to 3D has been slow to occur due to computational requirements (algorithmic and hardware). Each evolution in simulation capability has provided further insight into and understanding of the complexity associated with wire array ablation and dynamics. Each step is missing some integral piece of the physics that impacts the net radiation output, asymmetries, etc. Valuable insight has been gained from these simulations, which makes these approaches useful despite their limiting assumptions.

To date, simulations have not been able to capture the phenomena seen experimentally due to limitations in the

[a)]Paper BI2 2, Bull. Am. Phys. Soc. **48**, 20 (2003).
[b)]Invited speaker.

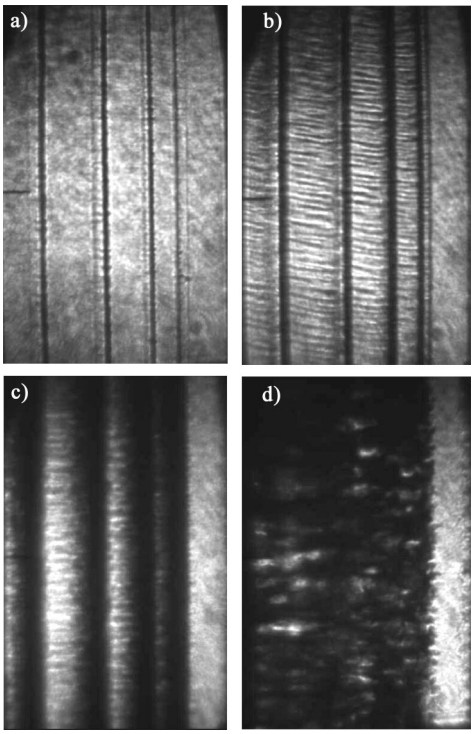

FIG. 1. Laser shadowgraph images of time evolution of low-wire number stainless-steel array (22-wire, Z1141, P. I. Brent Jones). Times shown are: (a) 2.440 μs, (b) 2.455 μs, (c) 2.470 μs, and (d) 2.486 μs.

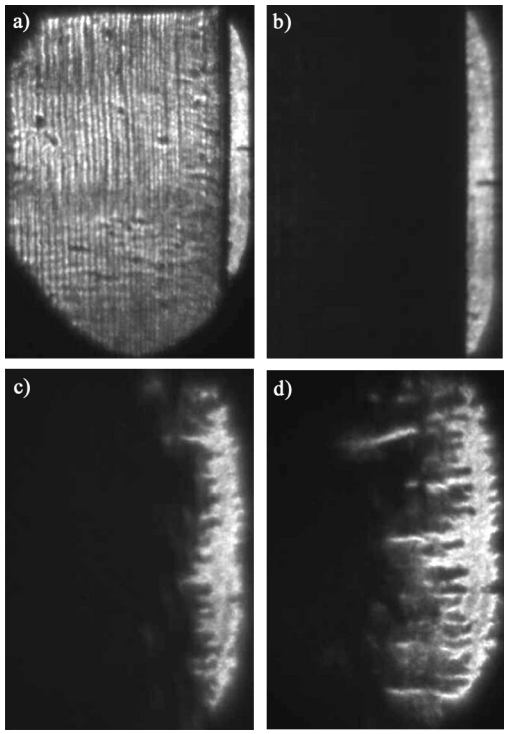

FIG. 2. Laser shadowgraph images for high wire number tungsten array (300-wire, Z1175, P. I. Dan Sinars). Times shown are: (a) 2.442 μs, (b) 2.462 μs, (c) 2.526 μs, and (d) 2.535 μs.

ability to accurately model the relevant geometries, assumptions of the material properties, initial conditions, and spatial resolution requirements. The purpose of this study is to further our understanding of wire array physics in 3D, attempt to reproduce the experimentally observed phenomena, and to discuss the limitations associated with modeling wire arrays in multiple dimensions. In Sec. II we describe the algorithms used to perform the simulations. Initial conditions for the simulations are discussed in Sec. III, followed by 2D simulations and discussion of their applicability in Sec. IV. Three-dimensional simulations are then presented in Sec. V with additional comparison to 2D simulation results. A brief summary is then presented in Sec. VI.

II. ALEGRA-HEDP

Sandia National Laboratories has developed a multiphysics research code tailored to simulate high energy density physics (HEDP) environments. ALEGRA-HEDP[16] has been used previously to simulate the evolution of wire arrays in 2D,[17,18] to examine wire initiation in one-dimensional (1D),[19] and simulate magnetic flyer plates for isentropic compression experiments.[20] To date it has produced the highest fidelity, 2D simulations of wire-array ablation and precursor plasma evolution.[17,18,21] The 3D version of ALEGRA-HEDP is now available and provides us with the ability to simulate the inherent 3D structure of wire ablation and array dynamics that is observed in experiments.

ALEGRA-HEDP uses an Arbitrary-Lagrangian-Eulerian (ALE) operator split algorithm to solve the resistive magnetohydrodynamic (MHD) equations as well as thermal and radiative transport. ALEGRA-HEDP originates from the ALEGRA code initially used for solid dynamics applications.[22] ALEGRA assumes that material motion can be described in terms of a Lagrangian step in which the various physical processes may be updated separately. The hydrodynamic approach is based on an explicit Lagrangian formulation to update the velocities and positions using a staggered formulation in space and time. An implicit magnetic diffusion formulation is used to update the magnetic field after the hydrodynamic motion of the material. After the Lagrangian steps have been performed, the remap portion of the ALE algorithm computes new values at new mesh locations. Mass, momentum, and energy are remapped using limited reconstruction algorithms based on a hexahedral mesh topology. The magnetic fluxes are remapped using a constrained transport algorithm to perform updates of the divergence-free magnetic-flux-density representation.

The implicit 3D magnetic diffusion discretization is based on a finite element formulation in which the discrete representation of the electric field utilizes low-order hexahedral edge elements and the magnetic flux density is represented using low-order face elements. The implementation of this discretization is crucial to solution accuracy. ALEGRA-HEDP has the ability to simulate vaccum regions, using low values of conductivity for rapid diffusion of magnetic field. This ability allows us to avoid the usage of physics cutoffs found in other MHD codes. The matrices created using this approach typically have a high condition number associated with a singular stiffness matrix having a large discrete nullspace interacting with a mass matrix proportional to conductivity in domains with several orders of magnitude variations

in spatial resolution as well as electrical conductivity. In order to obtain an accurate and efficient solution to these types of matrices, an algebraic multigrid iterative solver was designed specifically for this type of discretization of the magnetic diffusion equation.[23]

Thermal and radiation transport models have been implemented and are essential for modeling energy transfer. The thermal transport discretization is a face-centered, support operator methodology. Thermal coupling is forced to be local since no algebraic multigrid is available. A nodal finite element discretization is used for radiation diffusion and an algebraic multigrid capability is available.

III. INITIAL CONDITIONS

In wire arrays like those fielded on the Z accelerator,[1–3] the early time pre-pulse current sufficiently heats the individual wires to above one eV, thus the wires melt, vaporize, and eventually convert to plasma, although not necessarily at once. The conversion of a single wire from solid-density room temperature to plasma is a complex process, involving multiple phase changes from solid, to liquid, to vapor, and eventually plasma. Indeed, in some instances a multi-phase liquid–gas foam structure is observed.[13,24,25] The simulation of such complex physics, the formation of nucleations sites or explosive boiling, for example, is not presented here. ALEGRA-HEDP is a single-phase, continuum approximation code and thus (in its present state) cannot simulate such phenomena. On the other hand, simulations of aluminum wire breakdown from cold solid to a core/corona structure do compare well with experiments[19] and prove useful in making good approximations of the initial conditions used here. During breakdown the time of corona formation and the energy deposited within each core are important, hence the most reasonable approach must be used.

The approach used to obtain the simulation initial conditions in this study was to start with a two-state initial condition consisting of a liquid core and a corona. The density and temperature of the two-state initial condition were chosen based on the evolution of single wire 2D RZ initiation calculations using the current drive (normalized appropriately per wire) in Fig. 3. For each of the Tungsten 1 cm radius wire array cases examined (30-, 90-, 300-, and 600-wire) the density started at nearly solid-density and the temperature was set to 0.5 eV ($\sim$5800 K). The initial diameter of each wire was 39.9 μm (30), 20.69 μm (90), 11.35 μm (300), and 8.0 μm (600). Corona was initialized out to 1.5$\times$ of the wire radius, with a temperature of 8.5 eV and a density four orders of magnitude below solid density. The material models used for this study were equation of state: ANEOS SESAME 3540, conductivites: Lee-More-Desjarlias (LMD)[26] for Tungsten, and XSN opacities for single-group radiation diffusion calculations.

The location of the initial conditions in material phase space (Fig. 4) places the wire cores just beyond the melt-transition along the vapor dome. The start time for each simulation was 2.37 μs, close to the beginning of the foot of the current pulse. Magnetic field was pre-diffused before the dynamics were initiated in order to obtain a proper solution for both the global and local magnetic field about the wires.

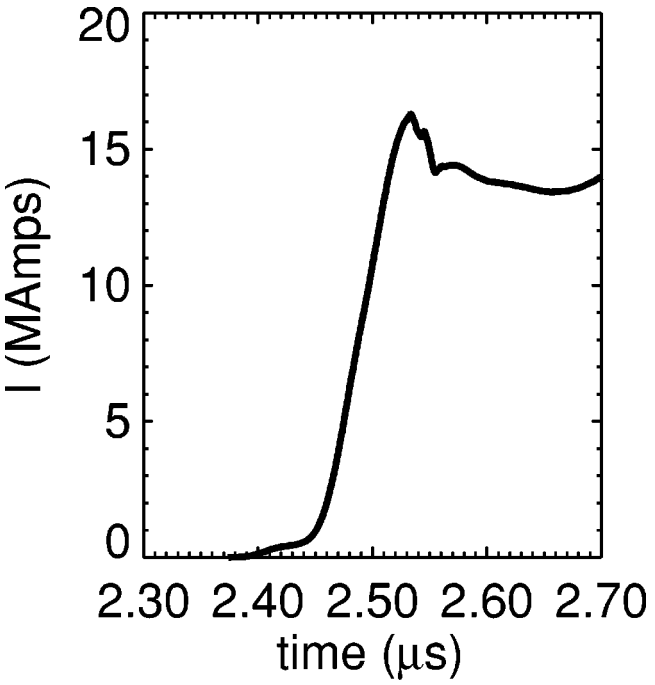

FIG. 3. Current drive used for simulations. The start time (2.450 44 μs) used for time scale normalization was computed by linearly extrapolating the linear current rise.

IV. 2D SIMULATION RESULTS

Three 2D simulations were performed in the x-y (r-θ) plane based on experiments performed by Mazarakis[27] on the

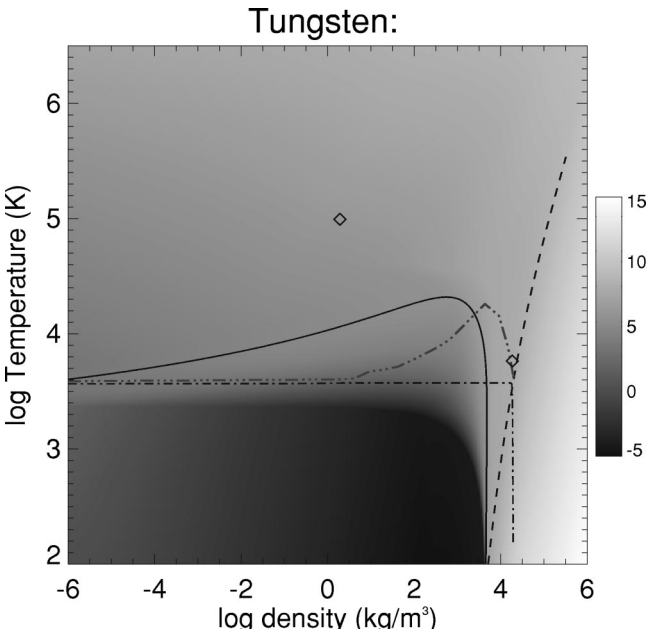

FIG. 4. Phase space plot for tungsten. Symbols plotted represent the core and corona initial conditions. Solid line: z-bar$=1$. Dashed line: Melt transition. Dash–dot line: Zero pressure. Dash–dot–dot–dot line: Vapor dome. The shading represents the log of the magnitude of the electrical conductivity (σ) in SI units.

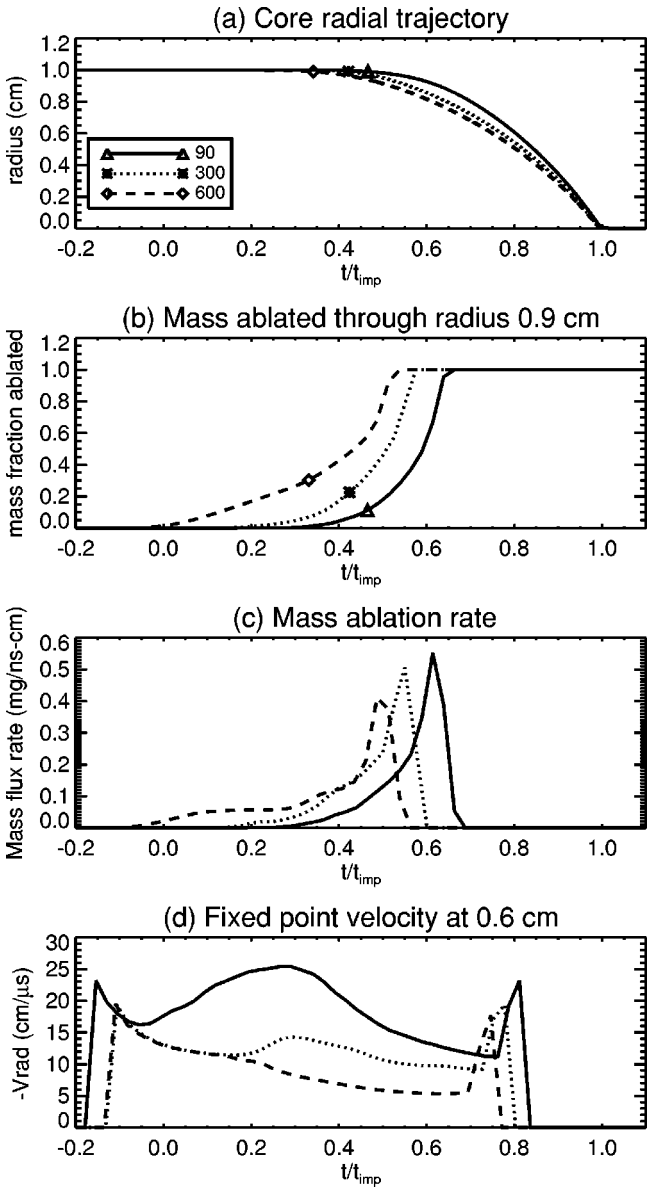

FIG. 5. Global temporal dynamics of the 90-, 300-, and 600-wire array 2D simulations: (a) Core radial trajectory, (b) total mass ablated, (c) mass ablate rate, (d) fixed point ablation velocity.

Z accelerator at Sandia National Laboratories. The time evolution of a single wire from each array was simulated on a wedge-shaped computational domain using reflection symmetry boundary conditions in the θ-direction. Using the initial conditions described in Sec. III, we successfully heated each wire using a current drive (see Fig. 3) applied at the radial boundary of the domain, creating precursor plasma that was swept toward axis by Lorentz forces before the remaining portion of the array stagnates onto the precursor. Because the simulation was 2D, no material was left behind (as seen experimentally), as it is suspected that this is only possible in 3D.

The global temporal evolution of each simulation (the trajectory of the wire core, mass ablated, mass ablation rate, and velocity past a point in the domain) is displayed in Fig. 5. The array core trajectory (computed using a Lagrangian tracer particle which follows the flow) was utilized to establish a normalized time scale based on a start time (linear extrapolation of current rise, see Fig. 3) and the final implosion time. All temporal examinations use this normalized time scale motivated by similar analysis of experimental data.[28,29]

The time of array motion was estimated when the core moves 1% away from its initial location. This point in time is represented as a plot symbol on each of the 90-, 300-, and 600-wire array trajectory curves [Fig. 5(a)]. The times of motion for each of the arrays are: 46% (90-wire), 42% (300-wire), and 34% (600-wire). This trend implies that the evolution of the wire array trajectory is becoming more shell-like (''0D'')[28] as wire number increases. The implosion times for each of the simulations were 2.552 μs (90), 2.550 μs (300), and 2.547 μs (600).

The time of motion symbols have also been placed in Fig. 5(b) to easily estimate the amount of mass ablated from the wire through the radius at 0.9 cm at the time of motion. The amount of mass ablated at the time of bulk array motion per array was: 11% (90-wire), 23% (300-wire), and 30% (600-wire). The corresponding mass ablation rates can be found in Fig. 5(c). These results suggest that the 600-wire case ablates more material early on, hence has more wire material ablated and earlier motion than the 300-wire and 90-wire cases. The 90-wire case, however, has the highest mass ablation rate overall.

Figure 5(d) displays the radial velocity of ablated material through a fixed spatial point placed at a radius of 0.6 cm. Clearly, the velocity of the material ablating from the wire does not remain constant. This is in contrast to the constant ablation velocity approximation used in the rocket equation,[28] but it is in agreement with the theoretical results of Oliver *et al.*[18] For the three simulations, the lower wire number case has the greatest radial velocity and the high wire number case has the lowest.

To further sample the ablated wire material, Lagrangian tracer particles were monitored through the simulations (see Fig. 6). Tracers were initially placed at the radial edge of the wire core closest to the array axis [Fig. 6(a)], a height of 1.05 r_{wire} above the wire core [Fig. 6(b)], a height of 0.8 r_{wire} above the wire core [Fig. 6(c)], and at the wire core itself [Fig. 6(d)]. The time evolution of the noncore tracers [Figs. 6(a)–6(c)] illustrates material that is rapidly accelerated and then tapers to an asymptotic value. The asymptotic values for Fig. 6(a) for the three wire arrays are 21 cm/μs (90), 15 cm/μs (300), and 4 cm/μs (600), which represents a nearly linear decrease in the asymptotic velocity reached [a similar linear decrease is seen for Figs. 6(b) and 6(c)].

All ablated material starts subsonic and rapidly accelerates to supersonic and even super-Alfvènic speeds[18] (not shown). Depending on the wire number of the array and the persistence of the local magnetic field, material can easily be accelerated to speeds of 10's of cm/μs ($\sim$Mach 10). The tracer in the wire core [Fig. 6(d)] demonstrates an initial delay as the wire ablates its exterior before the rapid rise to $\sim$50 cm/μs implosion velocity.

To complete the picture of the simulated 2D array dynamics for the 300-wire array spatial slices are plotted in Fig. 7 (the 90- and 600-wire cases show very similar evolution

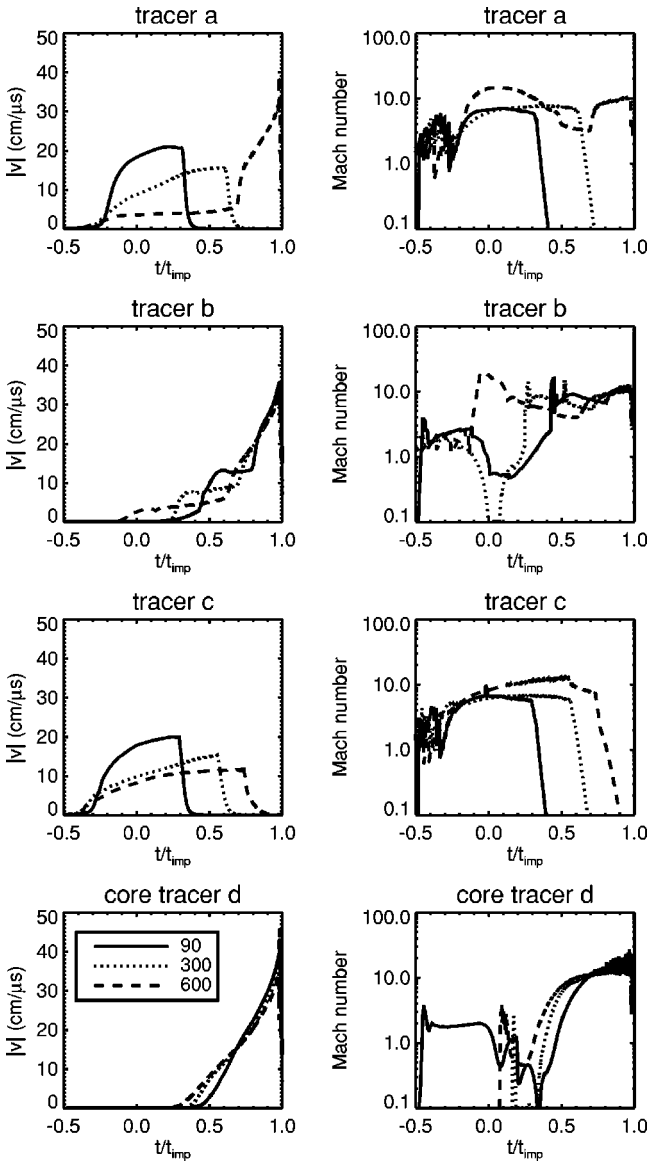

FIG. 6. Lagrangian tracer particle dynamics for tracers (a)–(d). The columns illustrate the material velocity, and the Mach number for each tracer.

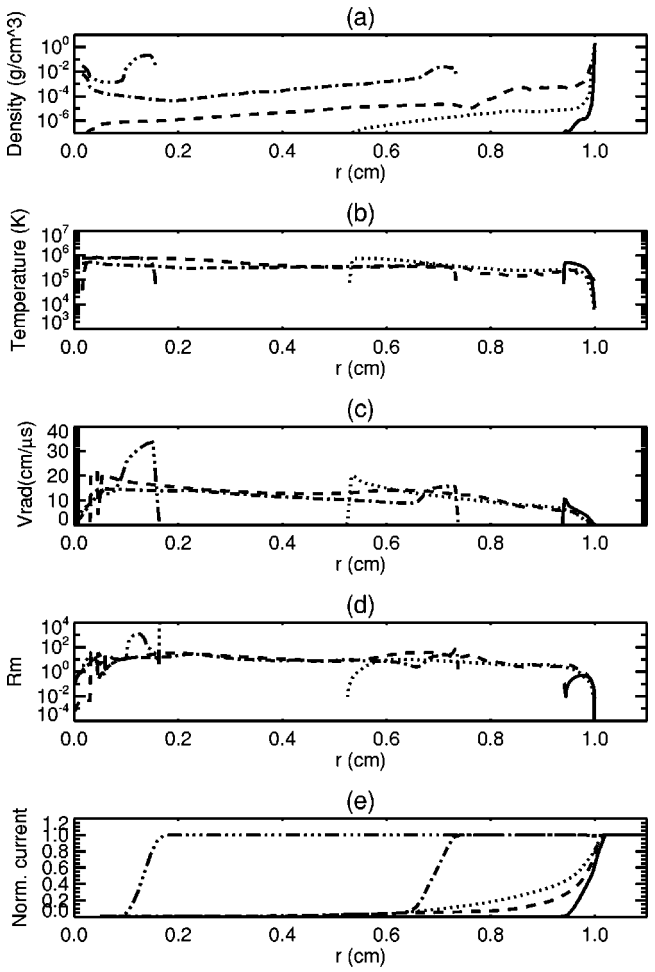

FIG. 7. Global spatial dynamics for the 90-, 300-, and 600-wire arrays: (a) Density, (b) temperature, (c) radial velocity, (d) magnetic Reynolds number, and (e) normalized current. Linestyles represent the following normalized times: 0.43 (solid), −0.05, (dotted), 0.27 (dashed), 0.7 (dash–dot), and 0.95 (dash–dot–dot).

hence are not shown). The density, temperature, radial velocity magnitude, magnetic Reynolds number, and normalized current along a radial cut of the simulation for the 300-wire array are shown. Figures 7(a) and 7(b) display the evolution of the low-density high-temperature coronal ablation and its acceleration toward axis. The core density drops nearly two orders of magnitude and stagnates onto the coronal precursor that has accumulated nearly four orders of magnitude in density. The velocity profile of the precursor and core are shown at various snapshots in time. Again, the ablated material accelerates as it travels toward axis, reaching a speed of ~ 20 cm/μs.

The magnetic Reynolds number (R_m), which estimates the extent to which magnetic field is ''frozen'' to the plasma, is displayed in Fig. 7(d). This quantity was computed via $R_m = \mu_0 \sigma v l$, where σ is the electrical conductivity, v the magnitude of the velocity, and l computed using $|\mathrm{B}|/curl(\mathrm{B})$ as an estimate of the length scale over with the magnetic field varies. The 3D wire ablation model proposed by Haines[30] suggests that the magnetic Reynolds number is somewhat less than unity, resulting in precursor plasma that does not advect current or magnetic field toward axis. The results from the 2D simulations indicate that the coronal material emanating from the wire core does in fact have R_m larger than unity downstream in the ablated flow. A normalized representation of the total current over time is presented in Fig. 7(e), which illustrates that between 5%–10% of the current is advected toward axis before the main implosion.

Results from the 2D simulations demonstrate that ablated wire material is both current carrying and the ablation velocity varies in both space in time. Using these simulations we assess the usefulness of the rocket equation and conclude that the rocket equation is reasonable provided one considers the ablation velocity to be representative of a time average flow velocity. In order for this to hold true, the temporal average of the ablated velocity needs to be relatively constant, which is supported by the simulations. A less restrictive derivation of the mass ablation rate similar to that in the rocket equation can be obtained using 1D theory,[18] avoiding the constraint of time-independence of the ablation velocity.

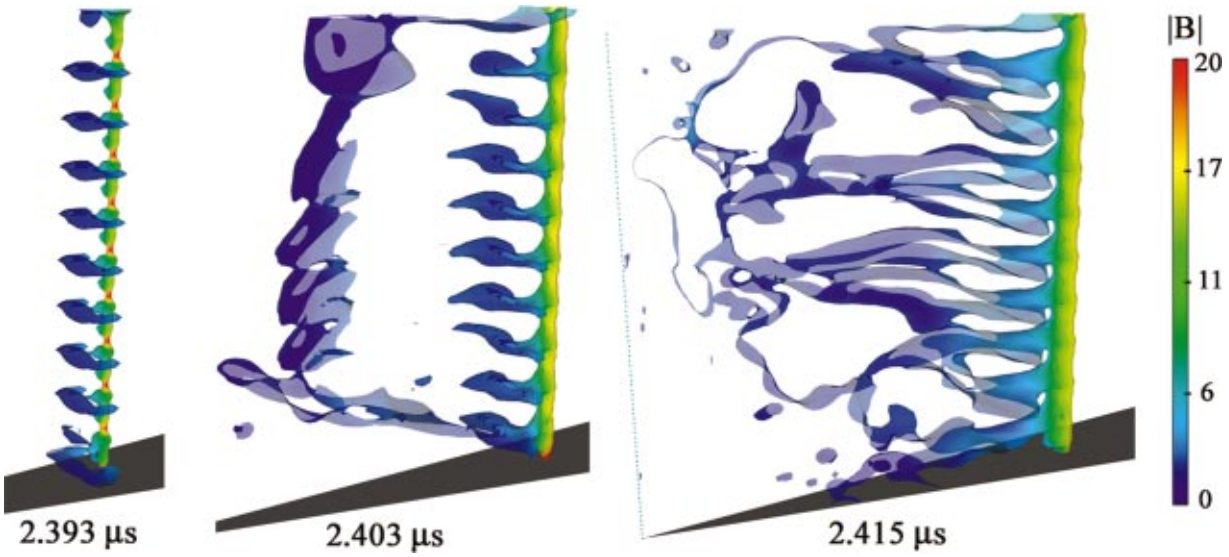

FIG. 8. (Color) Time evolution of 3D 30-wire simulation visualization using material boundary isosurface (containing core and coronal material) with magnetic field strength contour shading at times listed. The z direction is in the vertical direction.

Comparison of the radial trajectory of 2D simulations with experimental data shows a clear discrepancy. Radial trajectories for MAGPIE and the Z machine have a characteristic delay in the implosion, typically out to 60%–80% of the implosion time.[12,29] The 2D simulation results start to implode earlier, hence one may infer that the 2D simulated mass ablation rate is too high. This discrepancy is not necessarily related to the usage of incorrect initial conditions, rather it is more likely related to the fact that the actual experiment does not have a 2D evolution. Experimental data (see Figs. 1 and 2) clearly show a spatially varying mass ablation rate along the length of wires, whereas the 2D simu-

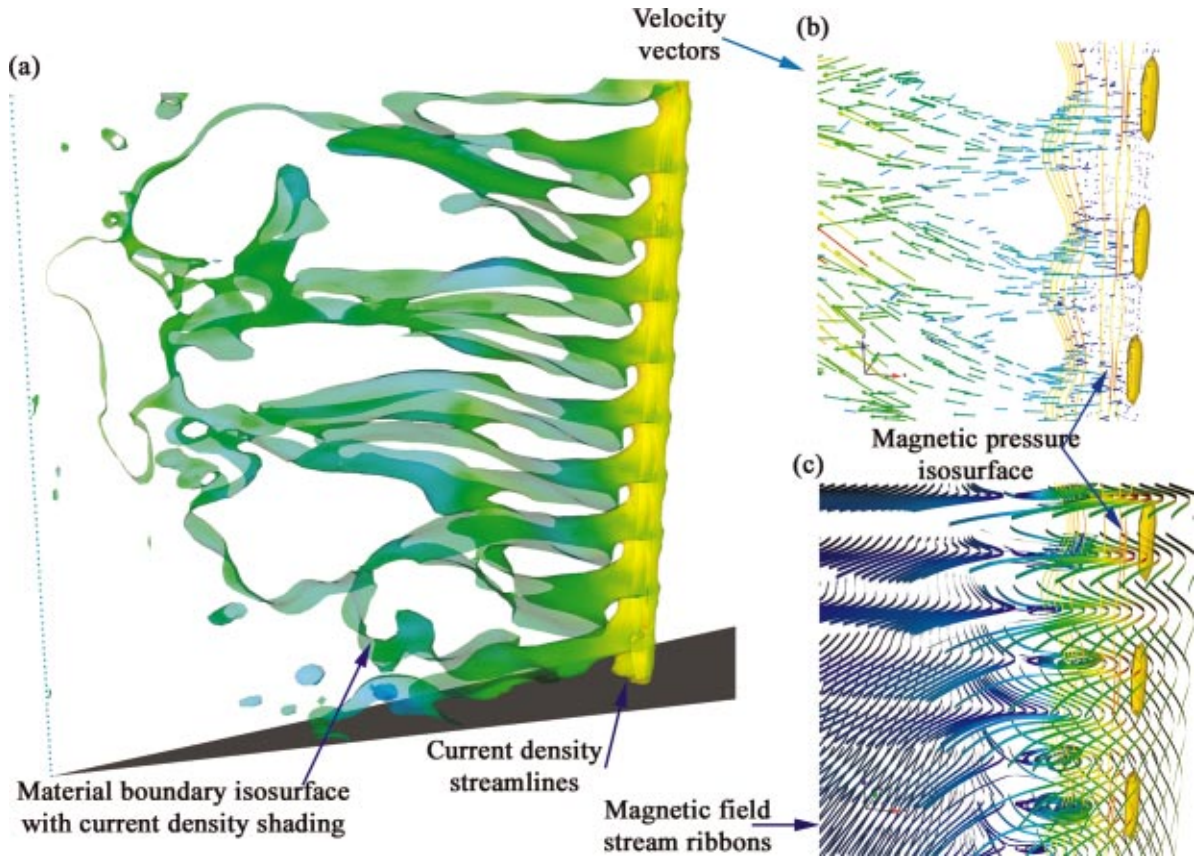

FIG. 9. (Color) Multiple views of wire array ablation: (a) Current density streamlines with material boundary isosurface logarithmically color shaded by magnitude of current density, (b) velocity vectors with current density streamlines and isosurface of magnetic pressure, (c) current density streamlines with magnetic pressure isosurface and magnetic field stream ribbons (shaded with strength of magnetic field) representing magnetic field morphology.

lations assume constant mass ablation, a clear source of overestimation. To help resolve this discrepancy, 3D simulations were run to quantify any reduction in mass ablation rate due to 3D effects.

V. 3D SIMULATION RESULTS

Recent experimental data from various Z-pinch accelerators provide evidence of the remarkable complexity associated with wire array initiation.[12–14] In addition to the 2D structure demonstrated in the r-θ plane, the wire ablation appears to have quasi-periodic structure in the axial (z) direction, with values ranging between 100 and 250 μm, depending on the wire material.[12] The seed for the perturbation is not well understood, possibly originating from various instabilities[30] or even from the wire extrusion process itself. Previous 3D numerical simulations have attempted to simulate wire array evolution, however, with limited spatial resolution.[11] The primary goal of this study was to attempt a 3D simulation of a single wire (again in a wedge-shaped geometry) and investigate the time evolution of the wire ablation using a fixed wavelength perturbation for an initial condition. A tungsten 30-wire array configuration was chosen based on experiments by Mazarakis[27] on the Z accelerator. The height of the array was 1 cm, and a ten-wavelength sinusoidal variation was used to perturb the wire core radius (maintaining constant wire mass/length) in the z direction to generate 3D variation.

The time evolution of a wire from the array is displayed in Fig. 8. The wire plasma is visualized using an isosurface that represents the outer surface of the wire material (core and corona) shaded with color contours of magnetic field strength for contrast. The sinusoidal perturbation applied creates smaller diameter necks of core material and an increased local magnetic field is generated. The enhanced local magnetic field at the necks generates increased Lorentz forces (magnetic pressure) that in turn causes coronal material formed at these locations to travel axially along the wire array. In contrast, the initially expanded regions are forced toward the array axis due to the global magnetic field and the resulting Lorentz forces acting on the material.

We suspect that this behavior is a variation to the $m=0$ instability with plasma columns in an array geometry. The images in Fig. 9 assist in verifying the model proposed, showing the development of well-defined material streams [Fig. 9(a)] off of the wire core. Figure 9(b) is the numerical analog to the simple sketch found in Haines[30] (Fig. 1), illustrating that as current is running about the core, the necked down regions have increased field strength (magnetic pressure isosurfaces) which cause material in the necks to be ''squeezed'' along the wire until they meet a region of inflow due to Lorentz forces associated with the global field. Figure 9(c) is a visualization of the morphology of the magnetic field shape as regions around the necks still have a null near the wire core, whereas the null is being advected toward axis in the ablation streams.

A second 3D simulation was run with no perturbation along the axial direction (hereafter ''2D''). Comparing the 3D simulation with the ''2D'' simulation, it is clear that the

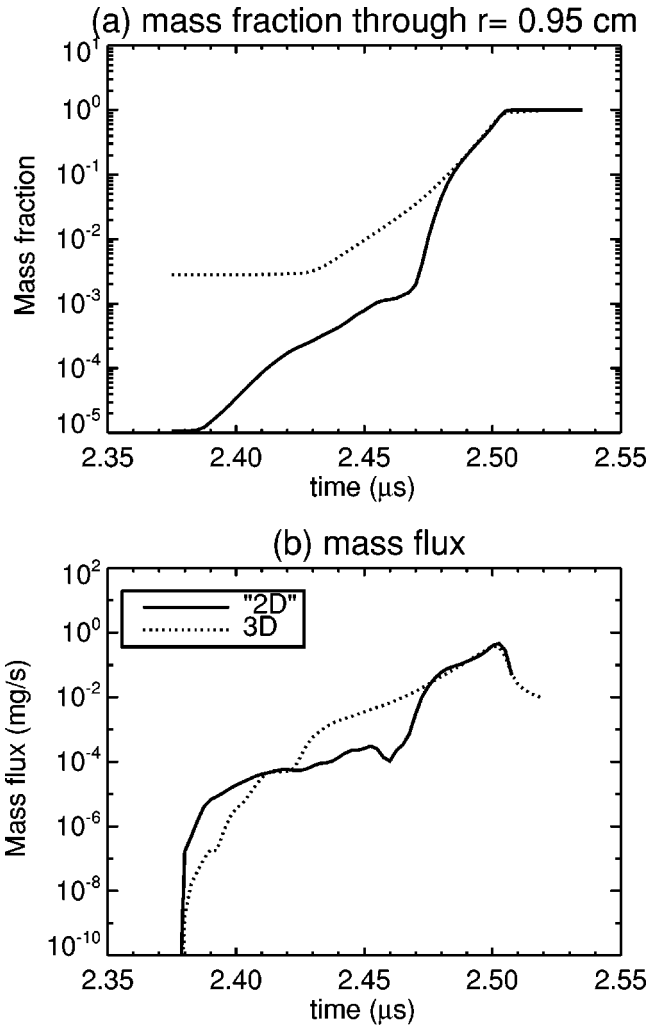

FIG. 10. Mass fraction and flux comparison between ''2D'' and 3D simulations.

3D simulation has an initial ($t<2.4$ μs) mass ablation rate which is reduced by a factor of 10–100 from that of the ''2D'' case (see Fig. 10). This effect is a result of the modified mass ablation due to the impact of the enhanced local magnetic field at locations along the axis of each wire. This result further supports the claim made in the previous section that 2D r-θ modeling of wire arrays is limited due to the symmetry assumption in the z direction.

The amount of current advected by the ablated material is compared for the ''2D'' and 3D simulations in Fig. 11. Just as the mass ablation rate is reduced in Fig. 10, so is the amount of current advected by the 3D wire evolution (by $\sim$5x). This is not to say that the R_m of the material has been reduced, rather that less material is actually ablated off the wire in comparison to the ''2D'' case. At times when ablated material has reached the axis, only a few percent of the total current has arrived. This supports experimental measurements made at MAGPIE.[12]

VI. SUMMARY

We have presented high-fidelity 2D and 3D simulations that provide insight into the time and spatial evolution of

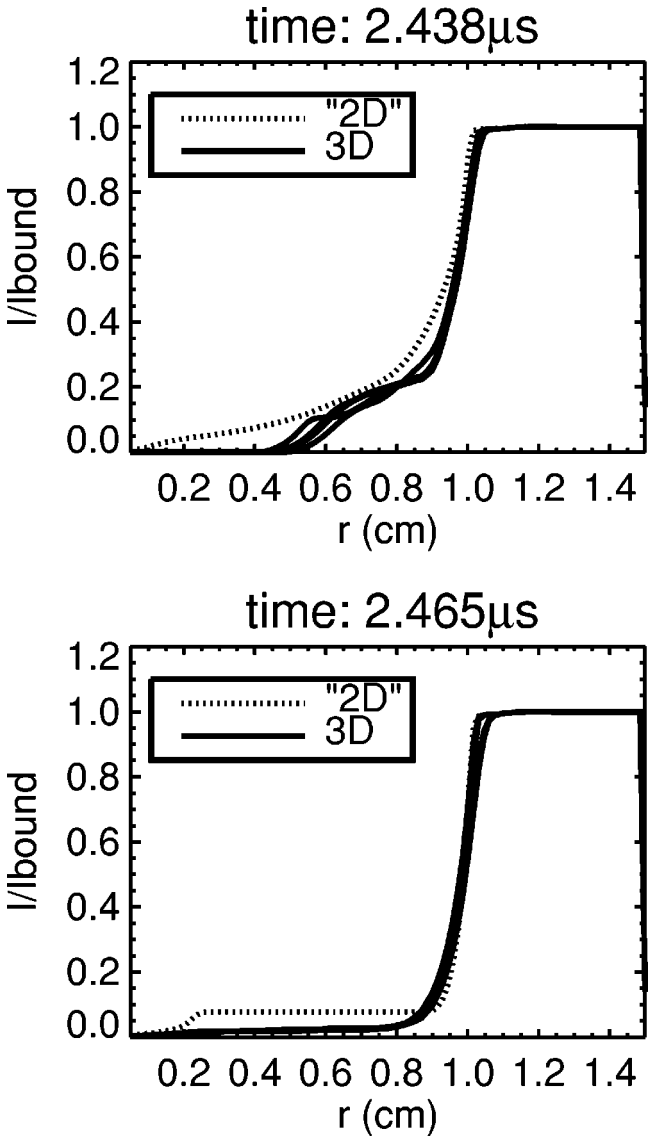

FIG. 11. Normalized current comparison (''2D'' vs 3D), times plotted are (a) 2.438 μs and (b) 2.465 μs. The multiple lines for the 3D case represents data from various z-positions in the domain.

wire ablation. It is clear that 3D effects impact the evolution of wire arrays and 2D simulations are insufficient to completely capture what is happening physically. The 3D simulations support the premise that the nonuniform axial ablation structure is maintained by the $m=0$ instability where the local field dominates in isolated areas along the length of the wire. Our simulations agree overall with the semianalytic model proposed by Haines[30] except with respect to the amount of current which the ablated material advects. Examining the magnetic Reynolds number for material downstream from the wire, we calculate a magnetic Reynolds number ~ 10. When comparing the total amount of current advected to axis, we find the 3D simulations have a reduced amount (~ 5x) with respect to the ''2D'' calculations, mainly due to the decrease in the amount of material actually traveling to axis. The 3D simulations has not evolved far enough in time to perform a comparison of the core trajectory with respect to the 2D simulation, however, from the amount of mass ablated and the ablation rate plotted in Fig. 10, one may infer that the wire plasmas will move at a later time in the 3D simulations than the ''2D.''

The perturbation used to initiate the 3D simulations involved a core perturbation. Usage of this perturbation was successful in establishing an axially varying mass ablation. We also attempted to vary the corona radius keeping the core radius fixed, however, we found that the perturbation information was advected away as the coronal material was swept to axis, rendering the evolution of the core nearly ''2D.'' Although the simulations do not allow us to address the seed of the perturbation in wire arrays, we believe that this study points us toward further examination of core instabilities,[31,32] rather than coronal perturbations.

The results from this study clearly support the need for further 3D simulations. Additional areas of investigation will include: (1) The impact of anomalous resistivity on the inflowing material and its impact on the amount of current advected by the precursor plasma; (2) usage of a circuit model rather than current drive in order to accurately model impedance changes on the computational domain which can then feedback to an external circuit;[19] (3) how array stagnation onto pre-fill influences radiation output in comparison with lower resolution models which do not accurately compute the formation or amount of precursor on axis before the main array implosion; and (4) the impact which current return structures might have on the plasma. With this information in hand, theory, models, and simulations will further bridge the gap in understanding between low- and high-wire number dynamics and performance. This will impact the future of radiation pulse-shaping, ICF, and the design of future machines at higher currents.

ACKNOWLEDGMENTS

The authors would like to thank the members of the ALEGRA-HEDP, ALEGRA/NEVADA, and AZTEC/ML teams for their continued support of this project as well as many useful discussions with Sergey Lebedev, Jerry Chittenden, Malcolm Haines, John DeGroot, Mike Cuneo, Mike Mazarakis, Dan Sinars, and Brent Jones.

Sandia is a multi-program laboratory operated by Sandia Corporation, a Lockheed Martin Company, for the United States Department of Energy's National Nuclear Security Administration under Contract No. DE-AC04-94AL85000.

[1] T. W. L. Sanford, G. O. Allshouse, B. M. Marder *et al.*, Phys. Rev. Lett. **77**, 5063 (1996).
[2] C. Deeney, M. R. Douglas, R. B. Spielman *et al.*, Phys. Rev. Lett. **81**, 4883 (1998).
[3] R. B. Spielman, C. Deeney, G. A. Chandler *et al.*, Phys. Plasmas **5**, 2105 (1998).
[4] M. K. Matzen, Phys. Plasmas **4**, 1519 (1997).
[5] R. Rosner, Bull. Am. Phys. Soc. **48**, 47 (2003).
[6] R. P. Drake, Bull. Am. Phys. Soc. **48**, 48 (2003).
[7] J. L. Porter, Bull. Am. Phys. Soc. **44**, 1948 (1997).
[8] T. J. Nash, M. S. Derzon, G. A. Chandler *et al.*, Phys. Plasmas **6**, 2023 (1999).
[9] D. L. Peterson, R. L. Bowers, W. Matuska *et al.*, Phys. Plasmas **6**, 2178 (1999).
[10] M. R. Douglas, J. S. DeGroot, and R. B. Spielman, Laser Part. Beams **19**, 527 (2001).
[11] J. P. Chittenden, S. V. Lebedev, S. N. Bland, F. N. Beg, and M. G. Haines, Phys. Plasmas **8**, 2305 (2001).

[12]S. V. Lebedev, F. N. Beg, S. N. Bland, J. P. Chittenden, A. E. Dangor, and M. G. Haines, Phys. Plasmas **9**, 2293 (2002).
[13]D. Sinars, M. Cuneo, D. Wenger, P. Rambo, I. Smith, and J. Porter, Bull. Am. Phys. Soc. **48**, 236 (2003).
[14]D. E. Bliss, G. S. Sarkisov, S. T. Rogowski, B. M. Jones, C. Deeney, T. J. Nash, K. W. Struve, and D. H. McDaniel, Bull. Am. Phys. Soc. **48**, 176 (2003).
[15]T W. L. Sanford, R. W. Lemke, R. C. Mock, and D. L. Peterson, Phys. Plasmas **10**, 3252 (2003).
[16]A. C. Robinson and C. J. Garasi, ''Three-dimensional *z*-pinch wire array modeling,'' Comput. Phys. Commun. (to be published).
[17]C. J. Garasi, K. Cochrane, M. P. Desjarlais, T. A. Haill, T. A. Mehlhorn, B. V. Oliver, and A. C. Robinson, Bull. Am. Phys. Soc. **47**, 243 (2002).
[18]B. V. Oliver, C. J. Garasi, T. A. Mehlhorn, and E. P. Yu, Bull. Am. Phys. Soc. **47**, 243 (2002).
[19]S. E. Rosenthal and M. P. Desjarlais, ''Equation of state and electron transport effects in exploding wire evolution,'' Proceedings of the IEEE International Pulsed Power Plasma Science Conference, June 2001.
[20]R. W. Lemke, M. D. Knudson, C. A. Hall, T. A. Haill, M. P. Desjarlais, J. R. Asay, and T. A. Mehlhorn, Phys. Plasmas **10**, 1092 (2003).
[21]E. P. Yu, T. A. Mehlhorn, Y. Maron, and D. Lepell, Bull. Am. Phys. Soc. **48**, 240 (2003).
[22]R. M. Summers, J. S. Peery *et al.*, Int. J. Impact Eng. **20**, 779 (1997).
[23]P. B. Bochev, J. J. Hu, A. C. Robinson, and R. S. Tuminaro, ''An improved algebraic multigrid method for solving Maxwell's equations,'' SIAM J. Sci. Comput. (to be published).
[24]G. S. Sarkisov, K. W. Struve, and D. H. McDaniel, Bull. Am. Phys. Soc. **48**, 175 (2003).
[25]S. A. Pikuz, T. A. Shelkovenko, V. M. Romanova, A. R. Migaleev, G. V. Ivanenkov, M. D. Mitchel, K. M. Chandler, B. M. Song, and D. A. Hammer, Bull. Am. Phys. Soc. **47**, 241 (2002).
[26]M. P. Desjarlais, Contrib. Plasma Phys. **41**, 267 (2001).
[27]M. Mazarakis, C. Deeney, M. Douglas *et al.*, Bull. Am. Phys. Soc. **48**, 176 (2003).
[28]S. V. Lebedev, F. N. Beg, S. N. Bland, J. P. Chittenden, A. E. Dangor, M. G. Haines, K. H. Kwek, S. A. Pikuz, and T. A. Shelkovenko, Phys. Plasmas **8**, 3734 (2001).
[29]M. E. Cuneo, G. A. Chandler, R. A. Vesey *et al.*, Bull. Am. Phys. Soc. **46**, 234 (2001).
[30]M. G. Haines, IEEE Trans. Plasma Sci. **30**, 588 (2002).
[31]M. D. Johnston, R. M. Gilgenbach, T. S. Strickler, Y. Y. Lau, M. C. Jones, T. A. Mehlhorn, and M. E. Cuneo, Bull. Am. Phys. Soc. **48**, 235 (2003).
[32]Y. Y. Lau, M. D. Johnston, R. M. Gilgenbach, T. S. Strickler, M. C. Jones, T. A. Mehlhorn, and M. E. Cuneo, Bull. Am. Phys. Soc. **48**, 235 (2003).